Observation of a different birefringence order at optical and THz frequencies in LBO crystal

Yu. M. Andreev[a,b,c], A. E. Kokh[d,e], K. A. Kokh[d,e], G. V. Lanskii[a,b,c], K. Litvinenko[f], A. A. Mamrashev[c,g], J. F. Molloy[h], B. Murdin[f], M. Naftaly[h,*], N. A. Nikolaev[c,g], V. A. Svetlichnyi[a,c]

[a] *Siberian PhysicalTechnical Institute of Tomsk State University, Tomsk, 634050, Russia*
[b] *Institute of Monitoring of Climatic and Ecological Systems SB RAS, Tomsk, 634055, Russia*
[c] *High Current Electronics Institute SB RAS, Tomsk, 634055, Russia*
[d] *Institute of Geology and Mineralogy SB RAS, Novosibirsk, 630090, Russia*
[e] *Novosibirsk State University, Novosibirsk, 630090, Russia*
[f] *Advanced Technology Institute, University of Surrey, Guilford, Surrey GU2 7XH, UK*
[g] *Institute of Automation and Electrometry SB RAS, Novosibirsk, 630090, Russia*
[h] *National Physical Laboratory, Teddington TW11 0LW, UK*

Abstract

THz optical properties of lithium borate (LBO) crystals were measured using time-domain spectroscopy (TDS). The LBO crystal samples were of high optical quality and were cut and polished along the ⟨100⟩, ⟨010⟩ and ⟨001⟩ axes. Two independent measurements were performed in order to confirm the reproducibility and consistency of results. The contradictions in the previously published data on the THz optical properties of LBO were clarified. It was shown that the birefringence order at THz frequencies is $n_z < n_x < n_y$, whereas at optical frequencies it is known to be $n_x < n_y < n_z$. It was seen that n_z, which has the highest value in the visible, has the lowest value at THz. This is explained in terms of ionic polarizability and is consistent with the fact that the THz absorption coefficient for a wave polarized along the Z-axis is more than an order of magnitude lower than for the X and Y axes. Absorption as low as 0.2 cm^{-1} was found at frequencies up to 0.5 THz for a wave polarized parallel to the Z-axis. A set of new dispersion equations was designed for the entire

*Corresponding author
Email address: mira.naftaly@npl.co.uk (M. Naftaly)

transparency range.

Keywords: lithium triborate, optical properties, terahertz generation

1. Introduction

Lithium triborate LiB_3O_5 (LBO) is an orthorhombic crystal belonging to the mm2 point symmetry group. In this work we use the convention labelling the optical axes as X, Y, Z, which in LBO are parallel to the principal crystallographic axes a, c, b [1]. LBO is a biaxial crystal which is known to have negative birefringence in its main transparency window of 155–3200 nm, i.e. $n_x < n_y < n_z$ (where the subscript indicates the crystal axis which is parallel to the polarization of the propagating wave). It is non-hygroscopic and chemically stable, has a moderate melting point of 1107 K [1], and Mohs hardness of between 6 and 7.2, allowing polishing with flatness up to $\lambda/10$ [2]. LBO is highly transparent between 500–1200 nm, with the absorption coefficient below 10^{-5} cm^{-1} [3, 4]. It has the highest surface damage threshold for laser radiation amongst all known nonlinear crystals, which is even higher than that of UV-grade fused silica [5]. The short wavelength of its transparency edge (155 nm) avoids multiphoton absorption under near IR laser excitation. This combination of favorable optical and physical properties, together with the possibility of phase matching, make LBO an attractive crystal for nonlinear applications. It is used widely for frequency conversion of high power lasers into the UV to near-IR, despite its low second order nonlinear susceptibility coefficients: d_{31}=0.67 pm/V, d_{32}=0.85 pm/V, and d_{33}=0.04 pm/V at λ=1.0642 μm ($d_{15} = d_{31}$, $d_{24} = d_{32}$) [1].

However, very little work has been published on the optical properties of LBO in the THz region, and there are no reports of THz applications. The only modeling data on normalized density of states in the 0–1500 cm^{-1} range is given in [6]. Some reflectivity and absorption spectra were published for 50–1800 cm^{-1} in [7]. Antsygin et al. [8] reported only two well-resolved dispersion curves (n_x and n_z) as well only two absorption spectra (α_x and α_z), omitting

the data for the Y-axis, apparently due to the low resolution of the available THz-TDS system. The relationship $n_z > n_x$ was found to be reverse to that seen in the visible. The measured birefringence was $n_z - n_x = 0.35$, and was estimated to be insufficient for phase matched THz generation [9].

Recently, a study aimed at verifying these results was performed on LBO crystals cut along the $\langle 100 \rangle$, $\langle 010 \rangle$ and $\langle 001 \rangle$ axes [9, 10], using a TDS system at the National Physical Laboratory, UK, described elsewhere [11]. Optically finished samples of flux-grown LBO crystals were manufactured by the same producer as for the previous study [8], the Institute of Geology and Mineralogy SB RAS, Russia [4]. It was found that the birefringence order at THz frequencies was in agreement with that at optical frequencies — i.e. $n_x < n_y < n_z$ — and was therefore contrary to $n_z > n_x$ reported in [8]. It was suggested that the result observed in [8] was occasioned by mistaken axis labeling. Moreover, the largest measured birefringence was $n_z - n_x = 0.42$, rather than 0.35 as reported in [8], which was ascribed to failure to observe the highest refractive index. The larger birefringence is particularly important because it places LBO amongst nonlinear crystals where phase matching is possible for down-conversion into the THz band.

2. Exprimental

LiB_3O_5 (LBO) cystals were grown from MoO_3 flux by modified Kyropoulos method [4, 12]. The charge from high purity H_3BO_3, Li_2CO_3 and MoO_3 was heated in Pt crucible to 900 °C for homogenization for 48 hr. Crystallization was started with a $\langle 001 \rangle$ oriented seed placed in contact with the melt at ≈750 °C. Then the temperature was decreased at the rate of 0.02–0.5 deg/hour; no pulling or rotation of the growing crystal was employed. The novelty of the employed growth method lies in its adoption of a non-symmetric distribution of temperature field inside the furnace [12]. Crystals of two thicknesses were used: 2 mm and 0.5 mm, measured with the accuracy of ±10 μm. LBO samples of different thicknesses and faces of 10×10 mm were cut along directions perpen-

dicular to the crystallographic axes a, b, c. The orientation was confirmed by X-ray diffraction data. Planes orthogonal to the a, b, c axes were determined in reference to the diffraction maximum of 1.154 Å radiation at the 2θ angle: 21.1° (hkℓ = (200)), 24.2° (hkℓ = (020)) and 34.9° (hkℓ = (002)). The optical axes X, Y and Z were set according to the generally accepted birefringence relation for LBO of $n_x < n_y < n_z$. The correspondence between the optical and crystallographic axes was determined to be X, Y, $Z \Rightarrow a$, c, b [1].

Two series of independent THz TDS measurements were performed in parallel at NPL, UK and IAE SB RAS, Russia. LBO samples were cut from the same single crystal boule and were identically finished. The largest crystal faces were cut normal to the $\langle 100 \rangle$, $\langle 010 \rangle$ and $\langle 001 \rangle$ crystal directions to within $10'$ of the crystallographic axis. The samples were optically finished, had high structural quality, excellent homogeneity, and very low optical absorption (10^{-5} cm^{-1}) at 500–1200 nm. Their orientations were identified independently by X-ray analysis prior to measurements and again afterwards. The two optical axes lying in the plane of crystal faces were labeled identically for both sets of samples.

Both TDS systems used for the measurements were laboratory-built. The TDS used at NPL & US was the same as that employed in the previous study [9], and was activated by a mode-locked Ti-sapphire laser with a center wavelength of 800 nm, pulse length of 20 fs, and average power of 400 mW. The system had been refurbished and improved by replacing some of the optical components, resulting in a greater measurement bandwidth than in [9]. The frequency resolution was 7.5 GHz, which was judged to be sufficient because the crystals lack absorption features. The TDS used by the IAE SB RAS was activated by a frequency-doubled mode-locked Er laser with a center wavelength of 775 nm, pulse length of 130 fs, and average power of 100 mW. The THz emitter was a high power multi-slit dipole antenna iPCA-21-05-1000-800-h (Batop GmbH, Germany), which replaced the one used in the previous study [8]. The TDS operation range was 0.1–4 THz, and the frequency resolution of the measurements was 12.5 GHz. Both TDS systems have a standard configuration employing 4 parabolic mirrors [13] (ch.1), and were tested and calibrated as

described in [13] (ch.6). In both sets of experiments, four measurement data sets were obtained for each crystal in each orientation; these were compared to confirm reproducibility, and the mean value was used for calculating the optical parameters.

The samples were positioned with high accuracy with the crystal face normal to the propagation direction of the polarized THz beam, with the beam polarization being parallel first to one and then the other crystal axis lying in the plane of the crystal face. The crystals were aligned normal to the THz beam by employing the back reflection of the probe beam, which is collinear with the THz beam. Figure 1 shows the time-domain traces of the recorded for the reference beam and for beams traversing the 2 mm thick crystal along three different axes. The measured refractive indices and absorption coefficients

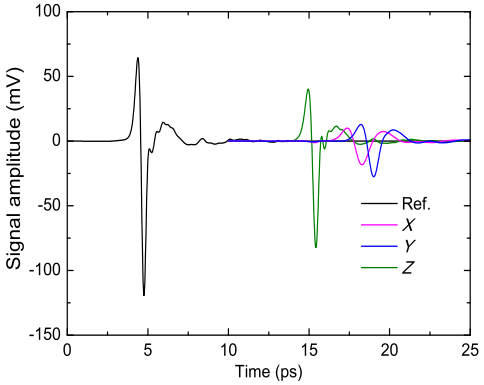

Figure 1: Part of time domain traces for reference and three crystal orientations, showing different delay and loss for beams travelling along different crystal axes.

were labelled x, y, z according to the crystal axis which lay parallel to the polarization of the THz beam (e.g. n_x for data where the beam was polarized along the X crystal axis). The refractive indices and absorption coefficients of the LBO crystals were calculated using standard procedures [13] (ch.2). Time-domain signals were recorded with no crystal in the beam path (reference) and transmitted through the crystal (sample). The spectral variation of the complex amplitude (i.e. field amplitude and phase) of both sets of data (reference and

sample) were obtained by applying Fourier Transform. The refractive indices n and absorption coefficients α of the crystal were calculated using equations [13] (ch.2):

$$H(\omega) = \frac{E_{sam}(\omega)}{E_{ref}(\omega)}, \tag{1}$$

$$n(\omega) = 1 - \frac{c}{\omega l} \arg H(\omega), \tag{2}$$

$$\alpha(\omega) = -\frac{2}{l} \ln \left(\left| H(\omega) \right| \frac{(1 + n(\omega))^2}{4n(\omega)} \right), \tag{3}$$

where ω is the angular frequency, and $\mathrm{E}_{sam}(\omega)$ and $\mathrm{E}_{ref}(\omega)$ are the complex amplitudes of sample and reference signals respectively, and l is a sample thickness. In the case of the 2 mm thick crystal, the Fabry-Perot echoes lay outside the time-domain data window. However, in the case of the 0.5 mm thick crystal, an iterative form of Eqs. 1, 2, 3 was employed in order to eliminate Fabry-Perot effects, as explained in [13] (ch.2). The uncertainties in the calculated optical parameters were evaluated as described in [13] (ch.4).

3. Results and discussion

Figure 2 plots the measured absorption coefficients $\alpha_{x,y,z}$, and refractive indices $n_{x,y,z}$; values at selected frequencies are listed in Table 1. Figure 2 shows three well resolved sets of data for the three crystal axes as measured by both IAE SB RAS and NPL & US, with the two sets of results being in good agreement in all cases. The most notable feature in Fig. 2a is that the birefringence order is confirmed to be $n_z < n_x < n_y$, and is different from that in the optical range which is $n_x < n_y < n_z$, as shown in Fig. 3. It is seen that n_z, which has the highest value in the visible, has the lowest value at THz. The previous THz data in [9] was found to have labelling errors in crystal axis assignment.

A different birefringence order in the visible and at THz is a highly unusual feature which may be explained by different magnitudes of electronic and ionic

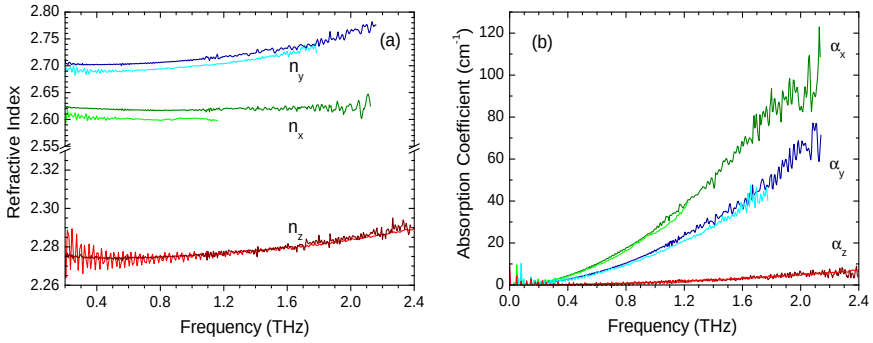

Figure 2: THz optical parameters measured at NPL & US (at 20 °C, cyan, green, red) and at IAE SB RAS (at 25 °C, blue, olive, brown). Subscripts denote crystal axis parallel to the polarization of the THz beam. a) Refractive index; b) absorption coefficient.

Table 1: THz refractive indices ($n_{x,y,z}$) and absorption coefficients ($\alpha_{x,y,z}$) measured by NPL (I line) and IAE (II line).

Frequency	n_x	n_y	n_z	α_x (cm^{-1})	α_y (cm^{-1})	α_z (cm^{-1})
0.6 THz	2.60±0.02	2.69±0.02	2.27±0.02	10±1	5.7±0.5	0.47±0.05
	2.618±0.007	2.704±0.006	2.274±0.005	10.16±0.03	6.05±0.02	0.47±0.02
1.0 THz	2.60±0.02	2.70±0.02	2.27±0.02	25±3	15±2	1.4±0.2
	2.618±0.007	2.710±0.006	2.275±0.005	26.91±0.06	16.40±0.04	1.37±0.03
1.2 THz	–	2.71±0.02	2.28±0.02	37±4	22±3	1.6±0.2
	2.620±0.009	2.717±0.006	2.278±0.005	38.35±0.08	23.57±0.06	1.80±0.03
1.5 THz	–	2.72±0.02	2.28±0.02	–	33±4	2.6±0.3
	2.62±0.01	2.73±0.01	2.279±0.005	58.70±0.09	35.08±0.08	2.56±0.06

polarizabilities. The Lorentz-Lorenz relation gives the refractive index in terms of microscopic polarizability [14]:

$$\frac{n^2-1}{n^2+2} = \frac{4\pi}{3}Np \tag{4}$$

where N is the number of molecules per unit volume and p is the atomic (or molecular) polarizability. At optical frequencies the polarizability p is purely electronic, but at THz frequencies it is often augmented by the addition of ionic component [15]. The presence of a Reststrahlen band in the crystal absorption (or reflection) spectrum — as is the case for LBO — lying between the opti-

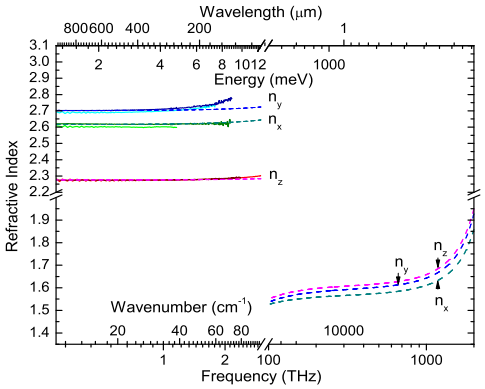

Figure 3: LBO refractive indices in the whole transparency range. Line colors and designations as in Fig. 2. Dashed curves were calculated from the developed dispersion equations.

cal and THz frequencies signals the onset of ionic polarizability, which causes the THz refractive index of such crystals to be higher than that in the visible. In birefringent crystals, however, the order of birefringence commonly remains the same for the optical and THz regimes. In this respect LBO is highly unusual. The cross-over points where the refractive indices coincide, $n_z = n_x$ and $n_x = n_y$, occur within the Reststrahlen band, where refractive indices exhibit anomalous dispersion due to phonon resonance absorption. The optical parameters in this region cannot be measured directly.

For LBO (mass density 2.474 g/cm^3), the molecular density is $N = 1.25 \times 10^{22}$ cm^{-3}. Polarizabilities can be calculated from equation (4) and are shown in Table 2. It is seen in Table 2 that the ionic polarizability component is significantly lower for a wave polarized along the Z axis than for the X or Y axes. It is also of interest that whereas for the X and Y axes the electronic and ionic polarizabilities are similar, for the Z axis the ionic polarizability is significantly lower than the electronic. The low ionic polarizability along the Z axis is also consistent with the very low absorption z, since absorption in polar dielectrics is mediated by the Debye mechanism [15]. In Fig. 2 the absorption coefficient z is at all frequencies (in the measured THz range) more than an order of magnitude lower than x and y. It is as low as 0.2 cm^{-1} at frequencies up to

Table 2: Polarizabilities calculated from equation (4).

	1.064 μm	1.0 THz	$p_{ionic} = p_{THz} - p_{opt.}$ (Å^3)
p_x (Å^3)	6.22	12.6	6.4
p_y (Å^3)	6.45	13.0	6.6
p_z (Å^3)	6.58	11.1	4.5

0.5 THz (similarly to that reported in [8]). These differences in the dielectric response of LBO for waves polarized along the Z axis and those polarized along X or Y axes may be ascribed to the complexity and asymmetry of the LBO crystal structure.

Dispersion equations for the entire transparency range of LBO were designed by using those for the maximal transparency window from [1] combined with the experimental data in Fig. 2(b), and by employing the procedure described in [9]; the results are plotted in Fig. 3:

$$n_x^2 = 2.453 + \frac{0.0119}{\lambda^2} + \frac{5.12\times10^{-5}}{\lambda^4} + \frac{4.2\times10^{-6}}{\lambda^6} + \frac{4.39\lambda^2}{\lambda^2-327} \tag{5a}$$

$$n_y^2 = 2.539 + \frac{0.0132}{\lambda^2} + \frac{7.12\times10^{-5}}{\lambda^4} + \frac{5.1\times10^{-6}}{\lambda^6} + \frac{4.76\lambda^2}{\lambda^2-246} \tag{5b}$$

$$n_z^2 = 2.589 + \frac{0.0122}{\lambda^2} + \frac{1.90\times10^{-4}}{\lambda^4} + \frac{3.3\times10^{-6}}{\lambda^6} + \frac{2.59\lambda^2}{\lambda^2-133} \tag{5c}$$

4. Conclusion

THz refractive indices and absorption coefficients of LiB_3O_5 crystals (LBO) for waves polarized along the X, Y and Z axes were measured using time-domain spectroscopy. LBO crystals of high optical quality were cut from a single ingot along the $\langle 100\rangle$, $\langle 010\rangle$ and $\langle 001\rangle$ crystal directions. The measurements were performed in parallel by two institutions: the National Physical Laboratory & University of Surrey, UK; and the Institute of Automation and Electrometry SB RAS, Russia. The results were seen to be in excellent agreement, clarifying the previous contradictions in the published data. It was demonstrated that the birefringence order at THz frequencies is $n_z < n_x < n_y$, whereas at optical frequencies it is known to be $n_x < n_y < n_z$. Whereas in the visible n_z has the

highest value, it is the lowest at THz frequencies. This is explained in terms of ionic polarizability and is consistent with the fact that the THz absorption coefficient for a wave polarized along the Z-axis is more than an order of magnitude lower than for the X and Y axes. Absorption as low as 0.2 cm^{-1} was found at frequencies up to 0.5 THz for a wave polarized parallel to the Z axis. A set of new dispersion equations was designed for the entire transparency range. LBO has the advantages of very high optical damage threshold, very low optical losses in the visible, absence of multiphoton absorption, and good thermal, thermo-optical and mechanical properties [1, 3, 4, 5, 9, 10], all of which make it an attractive crystal for nonlinear generation of THz radiation.

Acknowledgements

Russian Science Foundation (RSF) (15-19-10021) (crystal growth and approximation); Siberian Branch, Russian Academy of Sciences (VIII.67.3.2); EPSRC-UK ADDRFSS (EP/M009564/1); The National Measurement Office, UK.

References

[1] D. N. Nikogosyan, Nonlinear Optical Crystals: A Complete Survey, Springer-Verlag, New York, 2005. doi:10.1007/b138685.

[2] K. Kato, Tunable UV generation to 0.2325 μm in LiB_3O_5, IEEE Journal of Quantum Electronics 26 (7) (1990) 1173–1175. doi:10.1109/3.59655.

[3] N. Waasem, S. Fieberg, J. Hauser, G. Gomes, D. Haertle, F. Kühnemann, K. Buse, Photoacoustic absorption spectrometer for highly transparent dielectrics with parts-per-million sensitivity, Review of Scientific Instruments 84 (2) (2013) 023109. doi:10.1063/1.4792724.

[4] A. Kokh, N. Kononova, G. Mennerat, P. Villeval, S. Durst, D. Lupinski, V. Vlezko, K. Kokh, Growth of high quality large size LBO crystals for high energy second harmonic generation, Journal of Crystal Growth 312 (10) (2010) 1774–1778. doi:10.1016/j.jcrysgro.2010.02.023.

[5] Y. Furukawa, S. A. Markgraf, M. Sato, H. Yoshida, T. Sasaki, H. Fujita, T. Yamanaka, S. Nakai, Investigation of the bulk laser damage of lithium triborate, LiB_3O_5, single crystals, Applied Physics Letters 65 (12) (1994) 1480. doi:10.1063/1.112018.

[6] V. V. Maslyuk, T. Bredow, H. Pfnür, Phonon spectra and heat capacity of $Li_2B_4O_7$ and LiB_3O_5 crystals, The European Physical Journal B 42 (4) (2004) 461–466. doi:10.1140/epjb/e2005-00003-1.

[7] H. R. Xia, L. X. Li, H. Yu, S. M. Dong, J. Y. Wang, Q. M. Lu, C. Q. Ma, X. N. Wang, Structure and the nonlinearity of lithium triborate studied by Raman and infrared reflectivity spectroscopy, Journal of Materials Research 16 (12) (2001) 3464–3470. doi:10.1557/JMR.2001.0476.

[8] V. D. Antsygin, A. A. Mamrashev, N. A. Nikolaev, O. I. Potaturkin, T. B. Bekker, V. P. Solntsev, Optical properties of borate crystals in terahertz region, Optics Communications 309 (2013) 333–337. doi:10.1016/j.optcom.2013.08.014.

[9] Y. M. Andreev, M. Naftaly, J. F. Molloy, A. E. Kokh, G. V. Lanskii, V. A. Svetlichnyi, V. F. Losev, N. G. Kononova, K. A. Kokh, LBO: optical properties and potential for THz application, Laser Physics Letters 12 (11) (2015) 115402. doi:10.1088/1612-2011/12/11/115402.

[10] V. A. Svetlichnyi, M. Naftaly, J. F. Molloy, Y. M. Andreev, K. A. Kokh, G. V. Lanskii, N. G. Kononova, A. E. Kokh, Comments on "Optical properties of borate crystals in the terahertz domain", Optics Communications 365 (2016) 14–15. doi:10.1016/j.optcom.2015.11.046.

[11] J. F. Molloy, M. Naftaly, R. A. Dudley, Characterization of Terahertz Beam Profile and Propagation, IEEE Journal of Selected Topics in Quantum Electronics 19 (1) (2013) 8401508. doi:10.1109/JSTQE.2012.2205668.

[12] A. Kokh, V. Vlezko, K. Kokh, N. Kononova, P. Villeval, D. Lupinski, Dynamic control over the heat field during LBO crystal growth by High

temperature solution method, Journal of Crystal Growth 360 (1) (2012) 158–161. doi:10.1016/j.jcrysgro.2011.11.050.

[13] M. Naftaly, Terahertz Metrology, Artech House, 2015.

[14] M. Born, E. Wolf, Principles of Optics, Pergamon Press, Cambridge, 1980.

[15] S. O. Kasap, Principles of Electronic Materials and Devices, McGraw-Hill, New York, 2002.